Summary of the 2015/2016 Asian Winter Monsoon

31 May 2016
Tokyo Climate Center, Japan Meteorological Agency

This report summarizes the characteristics of the surface climate and atmospheric/oceanographic considerations related to the Asian winter monsoon for 2015/2016.

Note: Japanese 55-year Reanalysis (JRA-55; http://jra.kishou.go.jp/JRA-55/index_en.html; Kobayashi et al. 2015) atmospheric circulation data and COBE-SST (Ishii et al. 2005) sea surface temperature (SST) data were used for this investigation. The outgoing longwave radiation (OLR) data referenced to infer tropical convective activity were originally provided by NOAA. The base period for the normal is 1981 –2010. The term "anomaly" as used in this report refers to deviation from the normal.

1. Surface climate conditions

1.1 Overview of Asia

In boreal winter 2015/2016, general Asian climate characteristics included higher-than-normal temperatures in most lower latitudes as well as above- and below-normal precipitation over southeastern China to Japan and parts of the Maritime Continent, respectively. These conditions were largely consistent with expected El Niño winter patterns. Despite the prominent influence of the El Niño event, a severe cold wave associated with intra-seasonal variability struck East Asia in January.

Temperatures from December 2015 to February 2016 (DJF) were above normal in most parts of Asia and Siberia except for Mongolia and China (Figure 1.1). This tendency was especially apparent in low-latitude regions, and was consistent with typical anomaly patterns for past El Niño events (Figure 1.4). Meanwhile, extremely low temperatures were observed in Mongolia and China in January. A strong cold wave in late January was a notable weather characteristic of this boreal winter, which brought record-low temperatures and snowfall. In many regions, daily mean temperatures on January 24 were more than 6 degrees Celsius below normal (Figure 1.2).

Precipitation amounts averaged over DJF were below normal over the Maritime Continent and India (Figure 1.3). The dry conditions observed over the Maritime Continent were also consistent with typical anomaly patterns observed in past El Niño events (Figure 1.4). In most other regions, precipitation amounts were above normal in DJF. However, below-normal monthly precipitation amounts were observed in eastern Siberia in December, western to central Siberia and central to northeastern China in January, and from eastern parts of Central Asia to western China, southeastern China and the Indochina Peninsula in February.

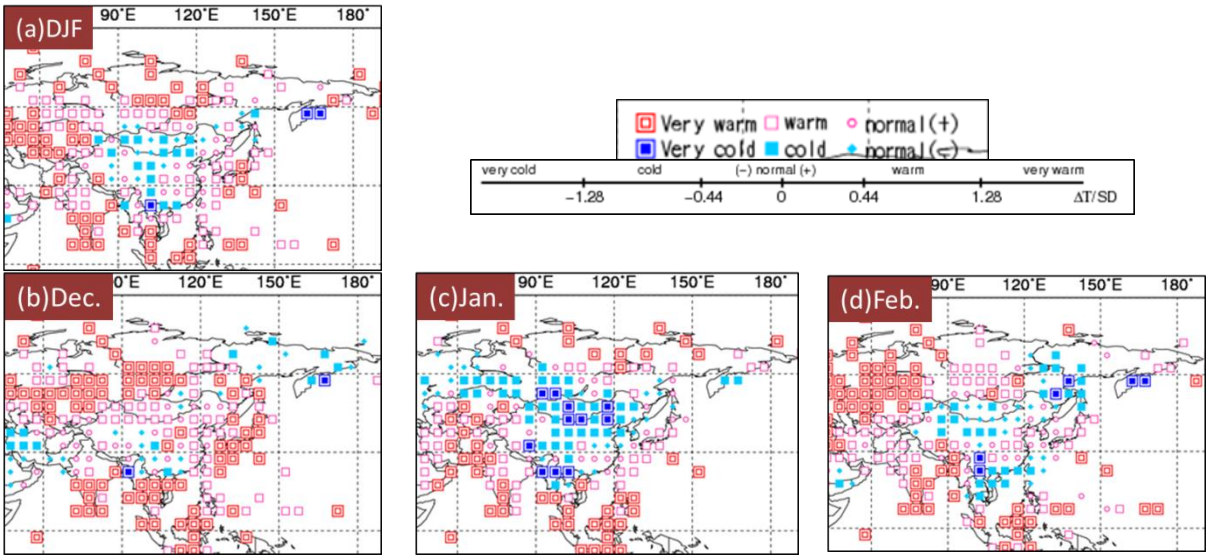

Figure 1.1 (a) Three-month mean temperature anomalies for December 2015 – February 2016, and monthly mean temperature anomalies for (b) December 2015, (c) January 2016 and (d) February 2016

Categories are defined by the three-month/monthly mean temperature anomaly against the normal divided by its standard deviation and averaged in 5° × 5° grid boxes. The thresholds of each category are -1.28, -0.44, 0, +0.44 and +1.28. Standard deviations were calculated from 1981 – 2010 statistics. Areas over land without graphical marks are those where observation data are insufficient or where normal data are unavailable.

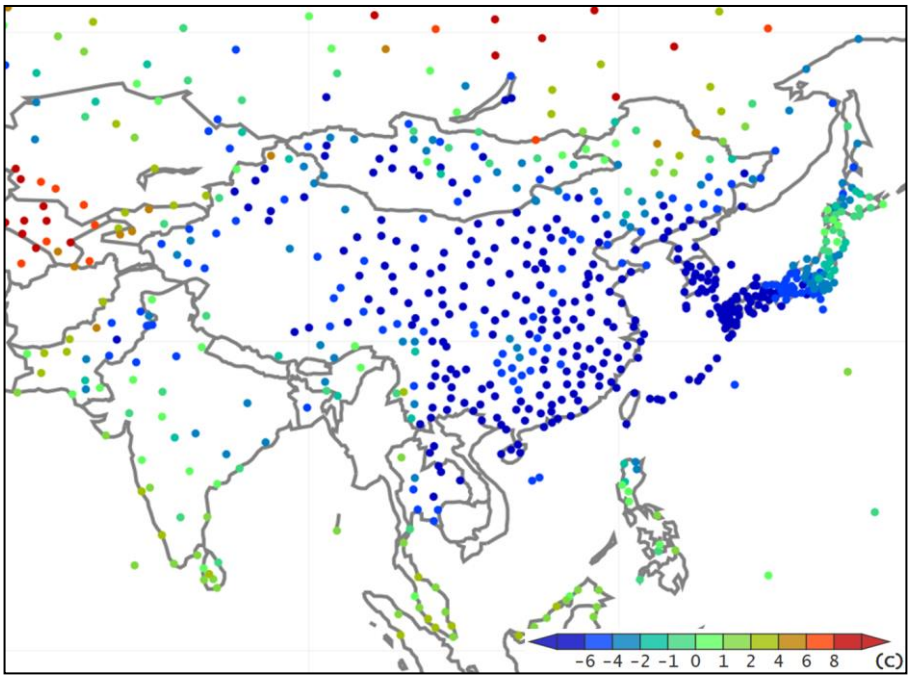

Figure 1.2 Daily mean temperature anomalies on 24 January 2016 based on SYNOP observation.

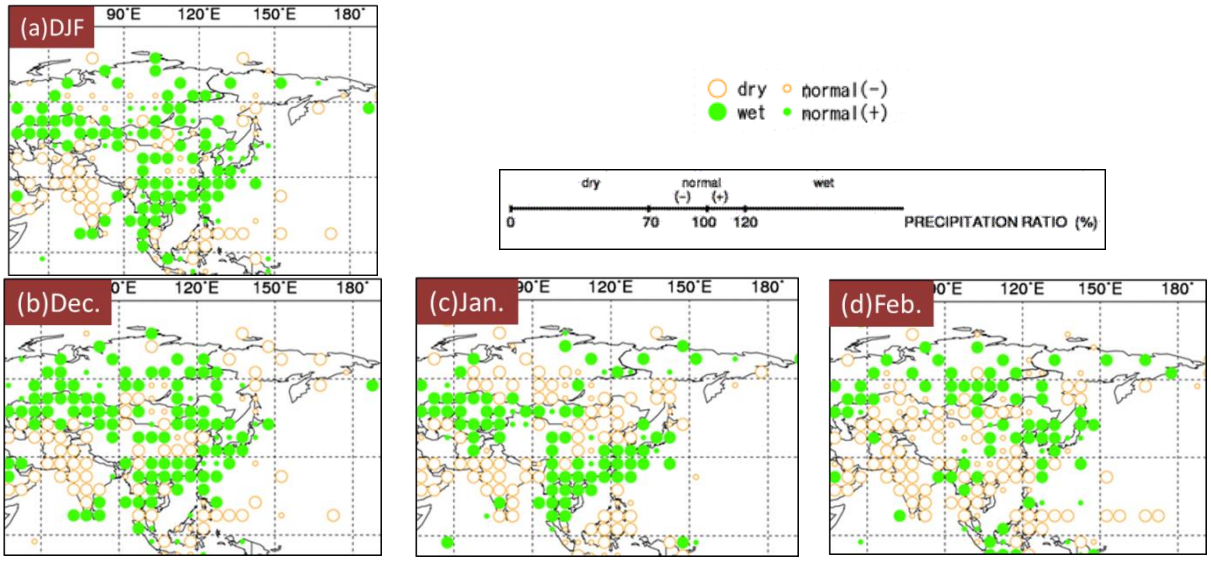

Figure 1.3 (a) Three-month total precipitation ratio for December 2015 – February 2016, and monthly precipitation ratio for (b) December 2015, (c) January 2016 and (d) February 2016

Categories are defined by the three-month/monthly mean temperature anomaly against the normal divided by its standard deviation and averaged in 5° × 5° grid boxes. The thresholds of each category are 70, 100 and 120%. Areas over land without graphical marks are those where observation data are insufficient or where normal data are unavailable.

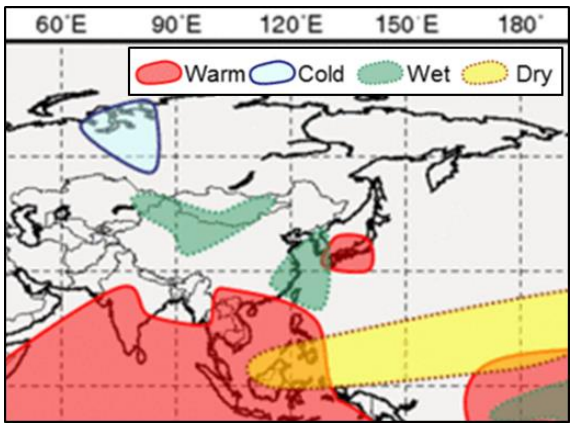

Figure 1.4 The schematic charts for typical anomaly patterns of surface temperature and precipitation in boreal winter in past El Niño events.

2. Characteristic atmospheric circulation and oceanographic conditions

2.1 Conditions in tropical SSTs and convective activity

In winter 2015/2016, the El Niño conditions that emerged in summer 2014 peaked. Sea surface temperatures (SSTs) were markedly above normal in the central-to-eastern equatorial Pacific and slightly below normal in tropical latitudes north of the equator in the western Pacific. In the Indian Ocean, SSTs were above normal basin-wide (Figure 2.1), as usually observed during or immediately after El Niño events. Although an active convection phase of the Madden-Julian Oscillation (MJO) propagated eastward from the eastern Indian Ocean via the Pacific and back to the Indian Ocean from early December to mid-January, eastward propagation of convection anomalies related to the MJO was limited (Figure 2.2) in association with the significant El Niño episode. Convective activity averaged over the three months from December to February, as well as for individual months, was enhanced over the central-to-eastern equatorial Pacific and suppressed over Southeast Asia (Figure 2.3).

2.2 Conditions in atmospheric circulation

In the 200-hPa stream function field (Figure 2.4 (a)), pronounced cyclonic circulation anomalies were centered over southern China in response to suppressed convective activity over Southeast Asia. Originating from this cyclonic circulation, a wave train pattern was noticeable with anticyclonic anomalies to the east of Japan. In the 850-hPa stream function field (Figure 2.5 (a)), anticyclonic circulation anomalies were centered over the Philippines and to the east of Japan. In relation, temperatures in the lower troposphere were above normal over and around Japan (Figure 2.7 (a)). Meanwhile, the Aleutian Low was stronger than normal southeastward of its climatological extension (Figure 2.8 (a)). Overall, the circulation anomaly pattern detailed above affords close parallels to those observed in past El Niño winters.

2.3 Notable events

In December 2015, the 500-hPa height field exhibited positive anomalies over Europe and East Asia and negative anomalies over the North Atlantic and Western Siberia (Figure 2.6 (b)). This pattern was reminiscent of circulation anomalies representing a negative phase of the Eurasian (EU) teleconnection pattern (Figure 2.9 (a)). This negative phase is generally linked to a weaker-than-normal Siberian High and higher-than-normal temperatures over East Asia, as observed in December 2015 (Figures 2.7 (b) and 2.8 (b)).

The phase of the EU teleconnection sharply reversed in early January and remained positive throughout the month (Figure 2.9 (b)) with a pronounced ridge centered over the longitude of 90°E and negative height anomalies over Eastern Europe and East Asia (Figure 2.6 (c)). This was in stark contrast to the circulation pattern dominant in the previous month. In close association with this change, the Siberian High turned stronger than normal (Figure 2.8 (c)), and temperatures were below normal over large parts of East Asia (Figure 2.7 (c)).

In late January, positive 500-hPa height anomalies over Western Siberia significantly amplified, and a deep trough concurrently developed over East Asia (Figure 2.10 (a)). In the lower troposphere between these positive and negative anomalies, the intensity and extension of the Siberian High increased (Figure 2.10 (b)) to a degree at which its center exhibited a rare sea level pressure exceeding 1,070 hPa. This created a situation in which a large part of East Asia was struck by an exceptional cold wave and experienced extremely low temperatures around January 23 – 24 (Figure 2.10 (c)). The outstanding intensity of the cold air outbreaks at that time can be evaluated using the method proposed by Iwasaki et al. (2014) in relation to cold-air mass anomalies and related horizontal flux. In this approach, the total cold-air mass below the potential temperature level of 280 K (approximately equivalent to the climatological potential temperature at 850 hPa zonally averaged along the latitude of 45°N in boreal winter) is calculated in terms of pressure difference between the ground and the 280-K level. On January 23, positive (i.e., above-normal) cold-air mass anomalies and northwesterly flux anomalies extended from eastern China toward western Japan (Figure 2.11 (a)). Six-hourly meridional flux anomalies of cold-air mass averaged over the 30 – 40°N and 110 – 130°E box reached their highest level since winter 1981/1982 (Figure 2.11 (b)), highlighting the unusual intensity of the late-January cold spell.

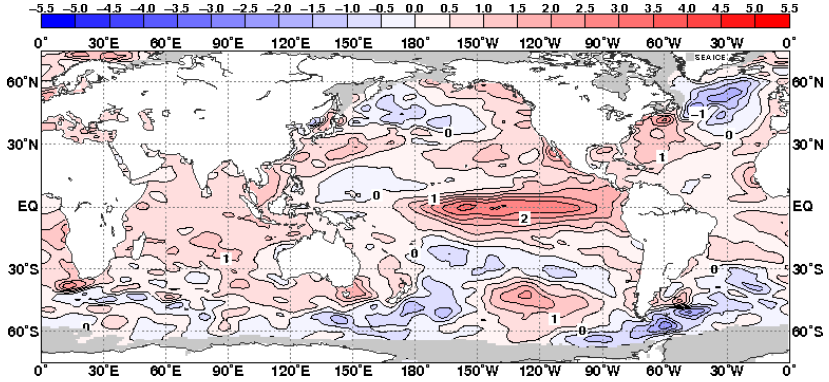

Figure 2.1 Three-month mean sea surface temperature (SST) anomalies for December 2015 to February 2016

The contour interval is 0.5˚C.

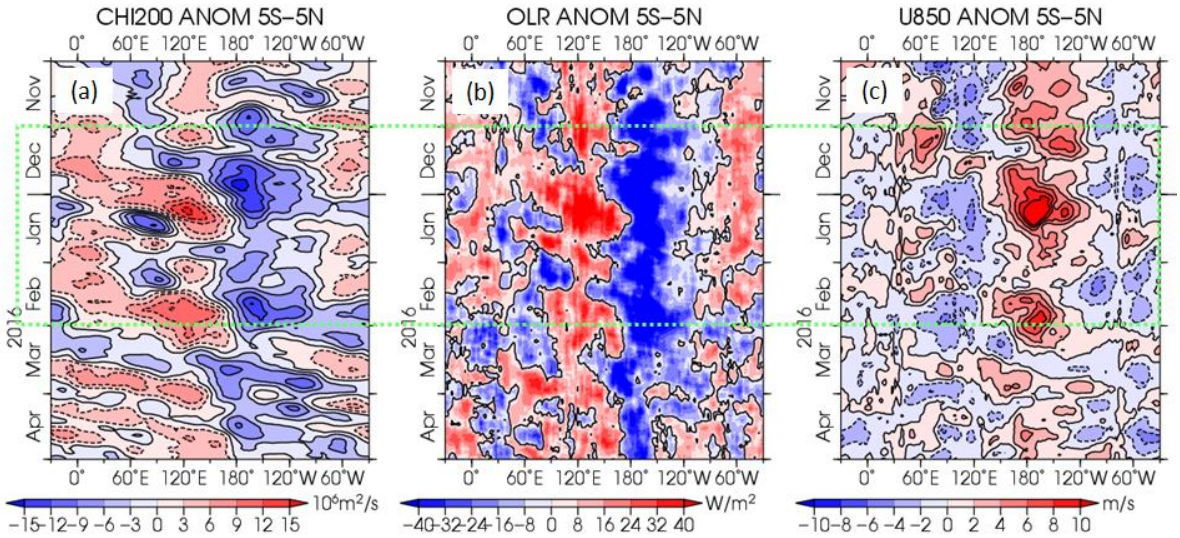

Figure 2.2 Time-longitude cross section of seven-day running mean (a) 200-hPa velocity potential anomalies, (b) outgoing longwave radiation (OLR) anomalies, and (c) 850-hPa zonal wind anomalies around the equator (5°S – 5°N) for November 2015 to April 2016

(a) The blue and red shading indicate areas of divergence and convergence anomalies, respectively. (b) The blue and red shading indicate areas of enhanced and suppressed convective activity, respectively. (c) The blue and red shading show easterly and westerly wind anomalies, respectively.

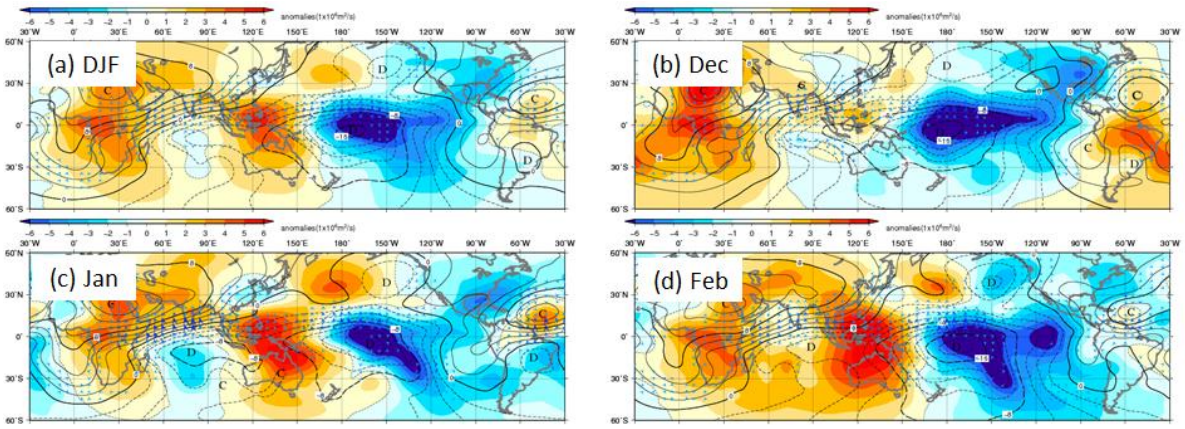

Figure 2.3 200-hPa velocity potential (a) averaged over the three months from December 2015 to February 2016, for (b) December 2015, (c) January 2016 and (d) February 2016

The contours indicate velocity potential at intervals of 2×10^6 m^2/s, and the shading shows velocity potential anomalies. D and C indicates the bottom and peak of velocity potential, corresponding to the centers of large-scale divergence and convergence, respectively.

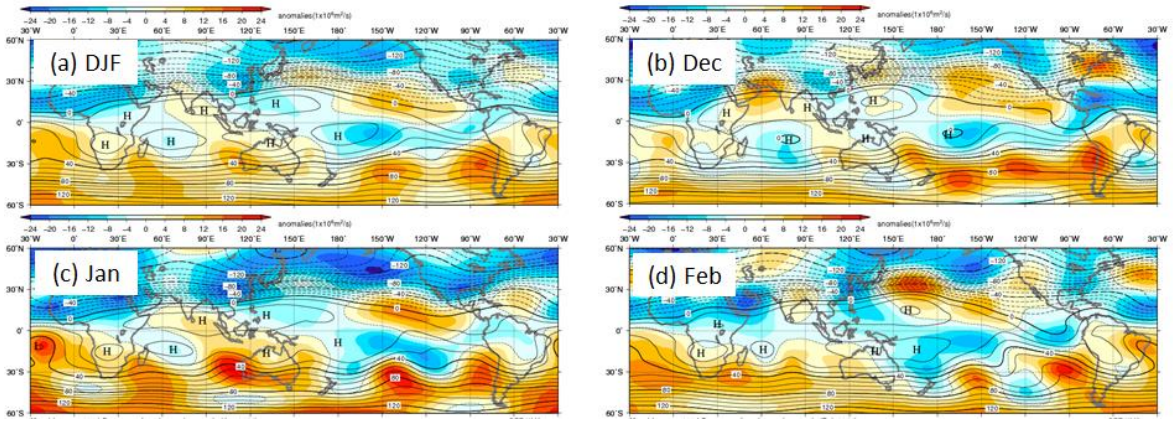

Figure 2.4 200-hPa stream function (a) averaged over the three months from December 2015 to February 2016, for (b) December 2015, (c) January 2016, and (d) February 2016

The contours indicate stream function at intervals of 10×10^6 m^2/s and the shadings indicate anomalies. H and L denote the centers of anticyclonic and cyclonic circulation anomalies, respectively.

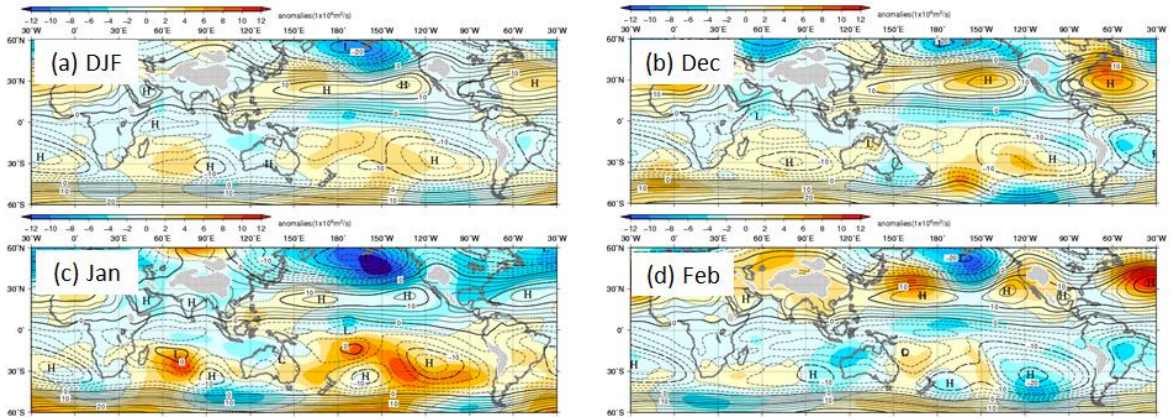

Figure 2.5 850-hPa stream function (a) averaged over the three months from December 2015 to February 2016, for (b) December 2015, (c) January 2016, and (d) February 2016

The contours indicate stream function at intervals of 2.5×10^6 m^2/s and the shadings indicate anomalies. H and L denote the centers of anticyclonic and cyclonic circulation anomalies, respectively.

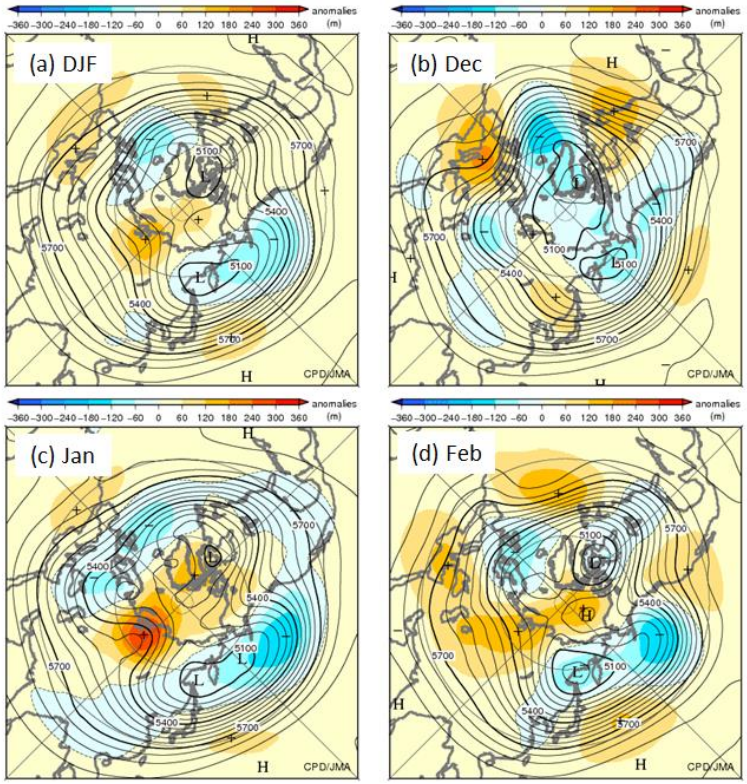

Figure 2.6 500-hPa height (a) averaged over the three months from December 2015 to February 2016, for (b) December 2015, (c) January 2016, and (d) February 2016

The contours indicate 500-hPa height at intervals of 60 m, and the shading denotes anomalies. H and L indicate the peak and bottom of 500-hPa height, respectively, and + (plus) and – (minus) show the peak and bottom of anomalies, respectively.

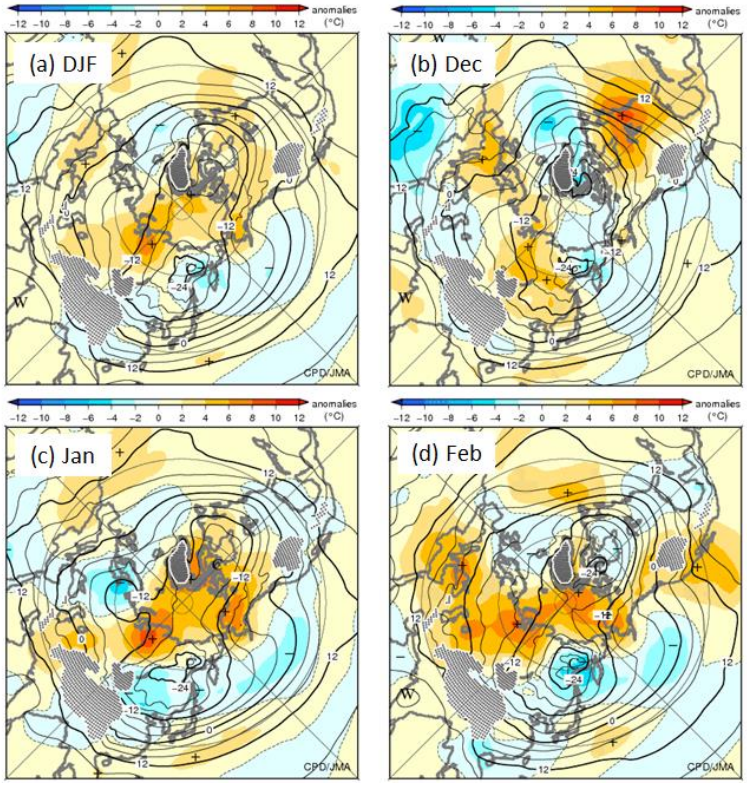

Figure 2.7 850-hPa temperature (a) averaged over the three months from December 2015 to February 2016, for (b) December 2015, (c) January 2016, and (d) February 2016

The contours indicate 850-hPa temperature at intervals of 4°C, and the shading denotes anomalies. W and C indicate the centers of warm and cold air, respectively, and + (plus) and – (minus) show the peak and bottom of 850hPa temperature anomalies, respectively.

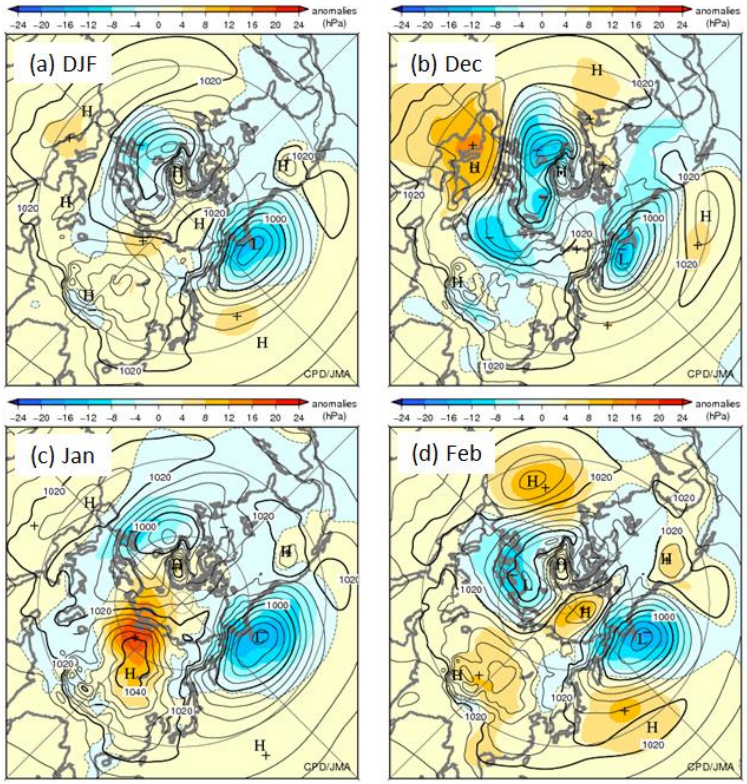

Figure 2.8 Sea level pressure (a) averaged over the three months from December 2015 to February 2016, for (b) December 2015, (c) January 2016 and (d) February 2016

The contours indicate sea level pressure at intervals of 4 hPa, and the shading shows related anomalies. H and L indicate the centers of high and low pressure systems, respectively, and + (plus) and – (minus) show the peak and bottom of sea level pressure anomalies, respectively.

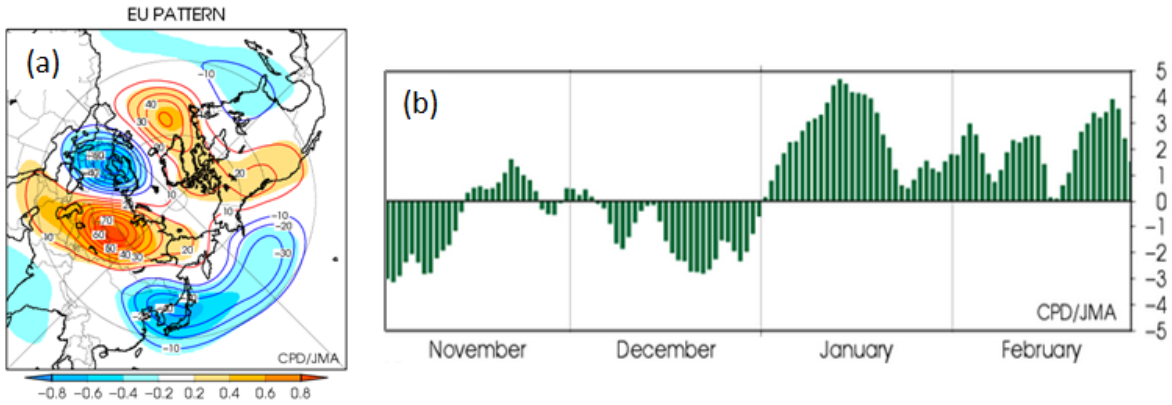

Figure 2.9 EU teleconnection pattern

(a) 500-hPa geopotential height anomalies regressed on EU pattern indices (contours) and correlation coefficients (shading). (b) Daily indices for November 2015 to February 2016.

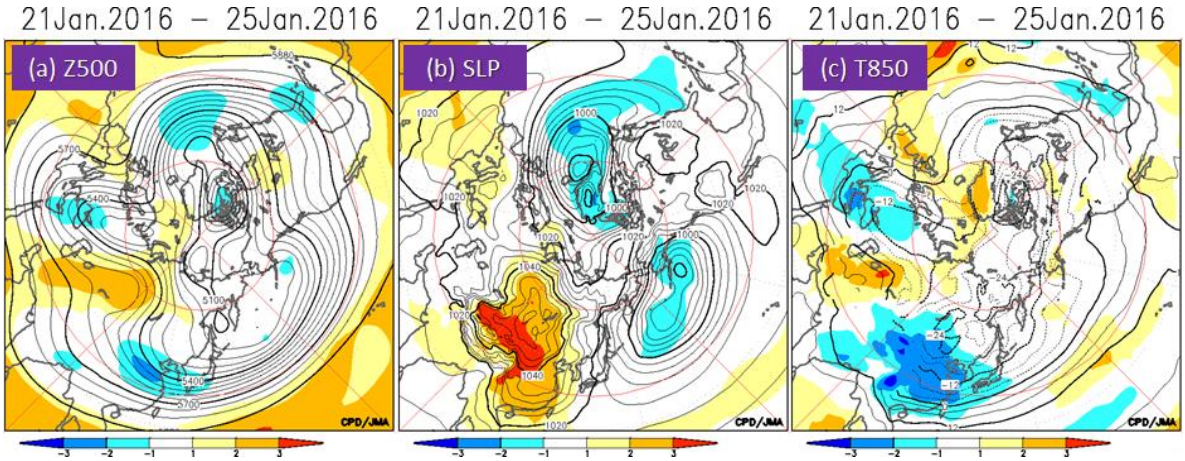

Figure 2.10 Circulation anomalies related to the exceptional cold wave which hit East Asia over the period of 21 – 25 January, 2016

The contours denote (a) 500-hPa height field, (b) sea level pressure field and (c) temperatures at 850-hPa. Shadings indicate related anomalies normalized by their standard deviations.

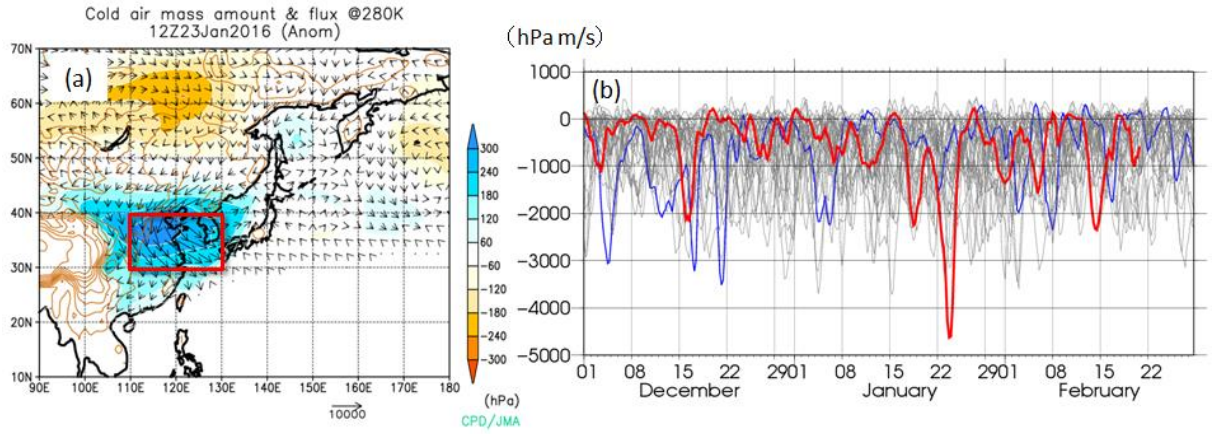

Figure 2.11 Intensity of cold-air masses and related flux

(a) Cold air mass amount (shading) and flux (arrows) anomalies on 12Z January 23, 2016. (b) Six hourly anomalies of cold air mass flux averaged over the box indicated in (a) for winter 2015/2016 (red), another recent cold winter 2005/2006 (blue) and other winters since 1981/1982 (grey).

(Yoshinori Oikawa and Kenji Kamiguchi, Tokyo Climate Center)

References

Ishii, M., A. Shouji, S. Sugimoto and T. Matsumoto, 2005: Objective Analyses of Sea-Surface Temperature and Marine Meteorological Variables for the 20th Century using ICOADS and the Kobe Collection. Int. J. Climatol., 25, 865-879.

Iwasaki, T., T. Shoji, Y. Kanno, M. Sawada, M. Ujiie and K. Takaya, 2014: Isentropic analysis of polar cold air mass streams in the northern hemispheric winter, *J. Atmos. Sci.*, **71**, 2230-2243

Kobayashi, S., Y. Ota, Y. Harada, A. Ebita, M. Moriya, H. Onoda, K. Onogi, H. Kamahori, C. Kobayashi, H. Endo, K. Miyaoka, and K. Takahashi, 2015: The JRA-55 Reanalysis: General Specifications and Basic Characteristics. *J. Meteorol. Soc. Japan*, **93**, 5 – 48.